Anisotropic Porous Materials for Drag Reduction

G26: Duke Bristow, Gianna Canto, Antoine Moats, Joe Rees

Dept. of Aerospace and Mechanical Engineering, University of Southern California.

USC Viterbi School of Engineering

Motivation

- Studies show that skin friction drag accounts for 50% of parasitic drag during cruise conditions for aircrafts [1].
- Drawing inspiration from biology, research on passive drag reduction has found that the jaggedness of shark scales, known as riblets, reduces circular flow along the surface leading to a decrease in friction.
- Further research estimates that reducing drag on aircraft by 1% may lead to a 0.5-1% reduction in fuel consumption depending on the aircraft [2].

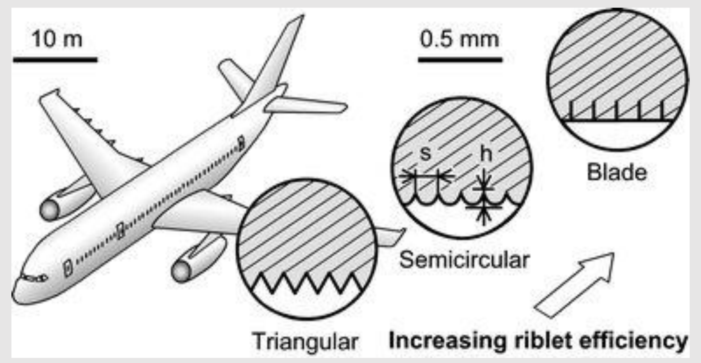

Figure 1. Theorized methods of drag reduction include riblets which vary in shape and size [3]

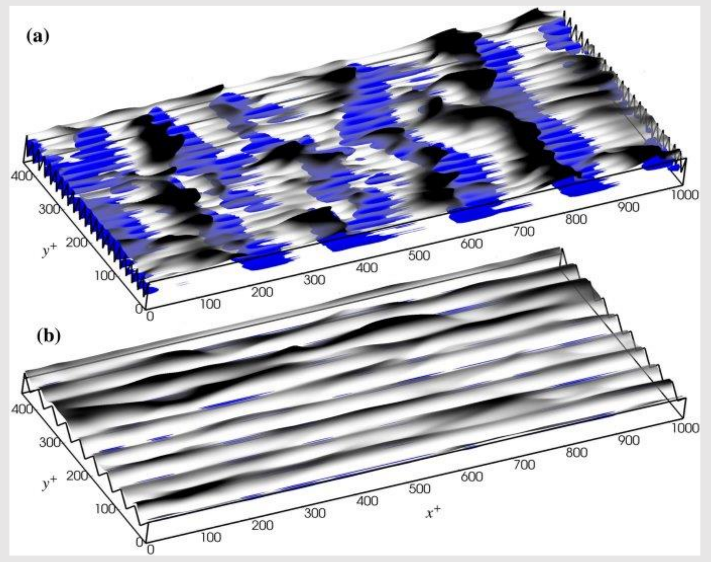

Figure 2. Diagram of the reduction of vortices (blue) as the riblet spacing changes [4]

- Riblets reduce drag by suppressing the development of circular flow in the spanwise direction, perpendicular to the flow, along the boundary [4].

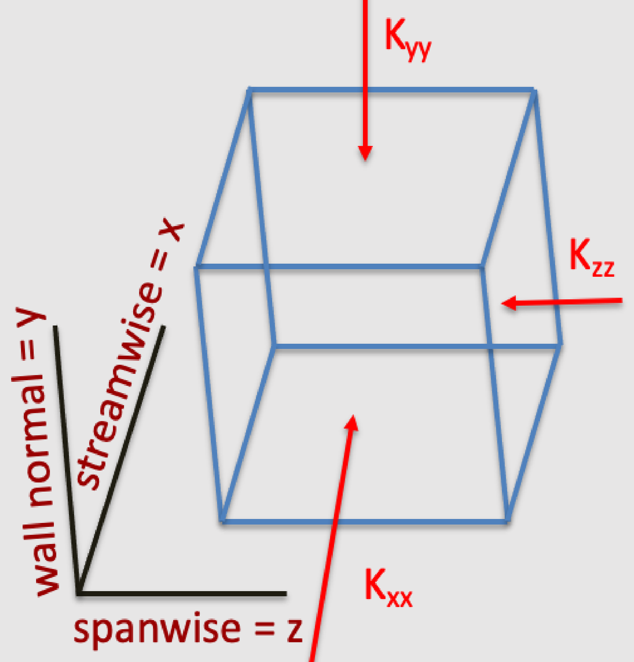

Figure 3: Flow directional diagram illustrating the permeability of the flow in each direction .

- Recent studies have demonstrated the reduction of vortices in both the spanwise and wall normal directions through the simulation of porous structures with permeability values (K_{xx}, K_{yy}, K_{zz}) shown in fig 2 [5]. These studies were pivotal in determining target permeability ratios (K_{xx} / K_{yy}) for drag reduction but not *specific geometries.*

- ***Goal: Determine permeability ratios and drag profiles through pressure drop measurements for Reynolds numbers of [500, 3000) for structured and unstructured geometries.***

Porous Structure Design

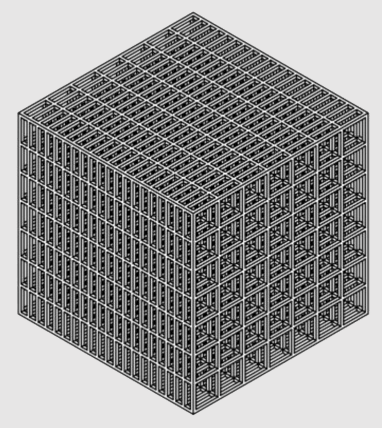

Figure 8. Cubic geometry cube for the permeameter setup based on previous experimental parameter sweeps for cubic porous structures.

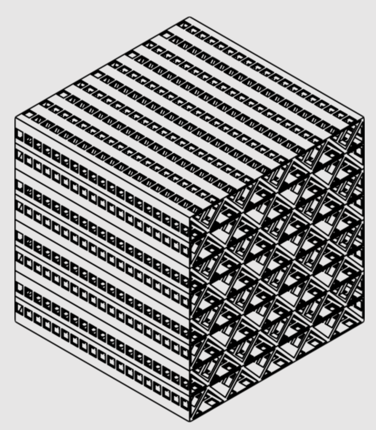

Figure 9. Riblet geometry cube for the permeameter setup based on previous porous drag reduction experiments manufactured using steel meshes

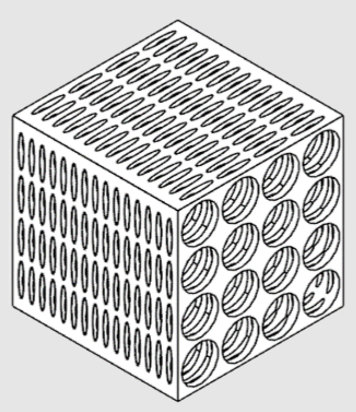

Figure 10. Elliptical geometry cube for the permeameter setup utilizing similar pore sizing as the cubic geometry. Chosen because the pore radius can be altered systematically

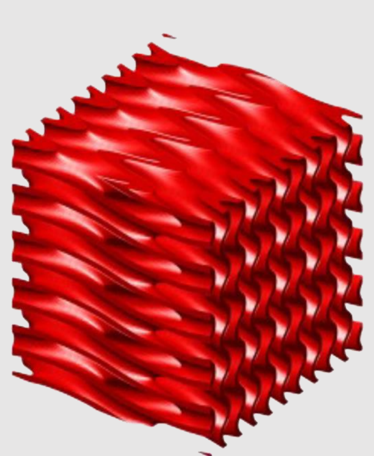

Figure 11 Gyroid permeability testing structure utilizing similar pore sizing as the cubic geometry. Chosen due to unique curvature and pore geometry.

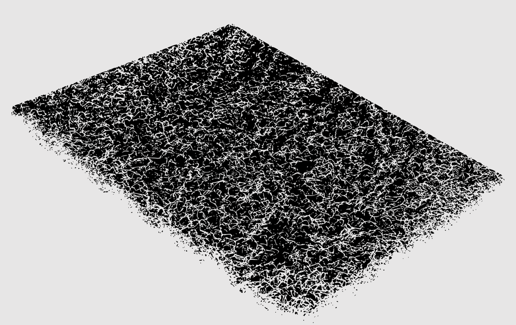

Figure 12. Commercial sponge pads of different pore sizes were used for a comparison to the structured geometries. Compared to the structured geometries, the geometry of these pads do not constitute a repeated pattern and instead are randomly assorted.

Experimental Setup

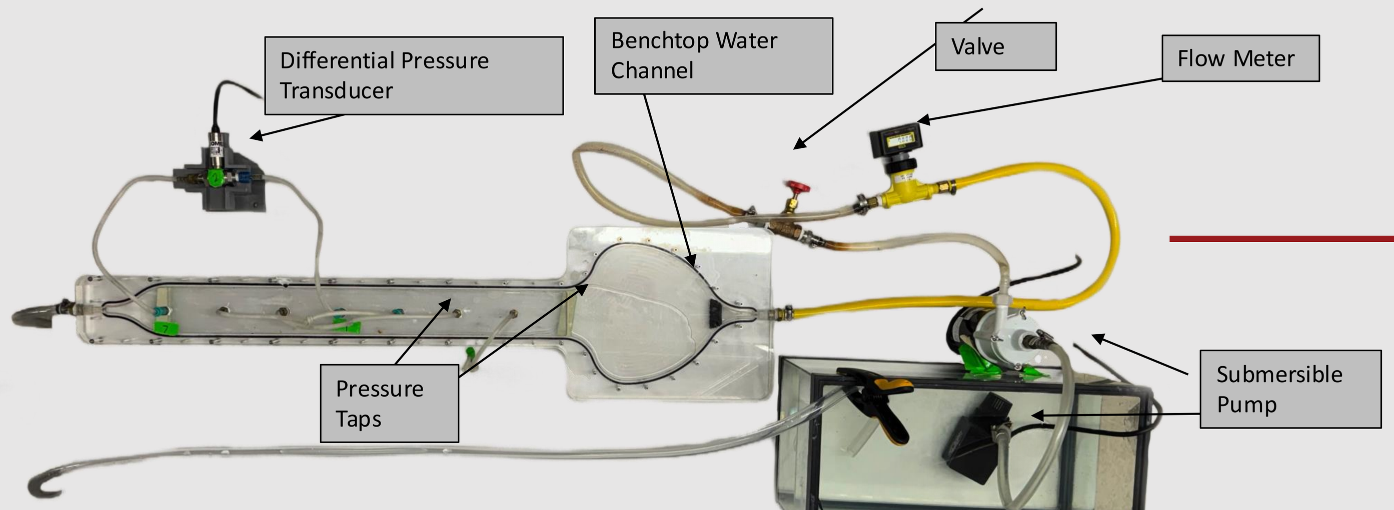

Figure 4. Working setup for the benchtop water channel.

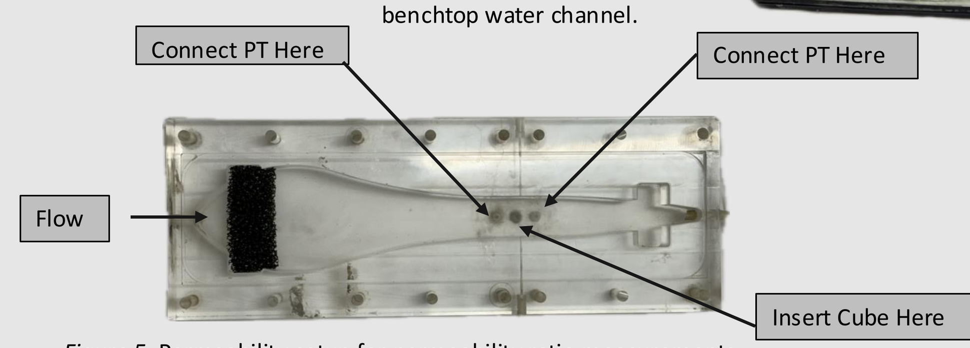

Figure 5. Permeability setup for permeability ratio measurements.

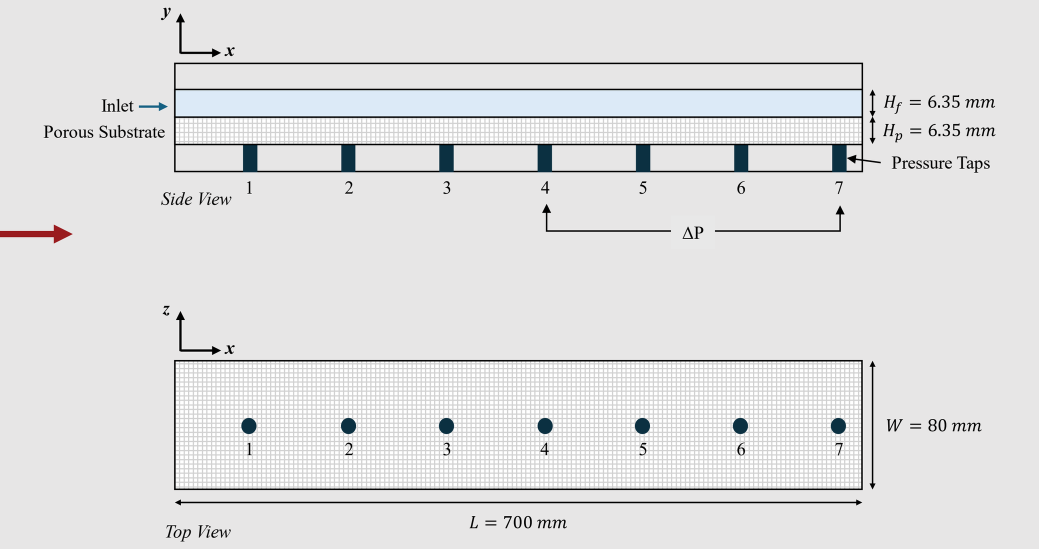

Figure 6. Benchtop water channel setup.

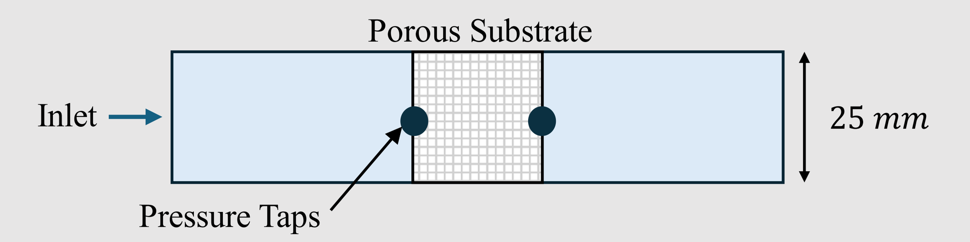

Figure 7. Permeameter setup for permeability measurements.

$$\boxed{\frac{dP}{dx} = \frac{v}{k_{xx}} U_b + CU_b^2}$$

Equation 1. Equation to determine friction factor, f, from the pressure gradient, $\frac{dP}{dx}$, bulk velocity, U_b, density of water, ρ, and the height of the unobstructed channel, H_f .

$$\boxed{f = \frac{dP}{dx}\frac{2H_f}{\rho U_b^2}}$$

Equation 2. Equation to determine the permeability ratio, k_{xx}, from the pressure gradient, $\frac{dP}{dx}$, bulk velocity, U_b, and the dynamic viscosity of water, v.

Results

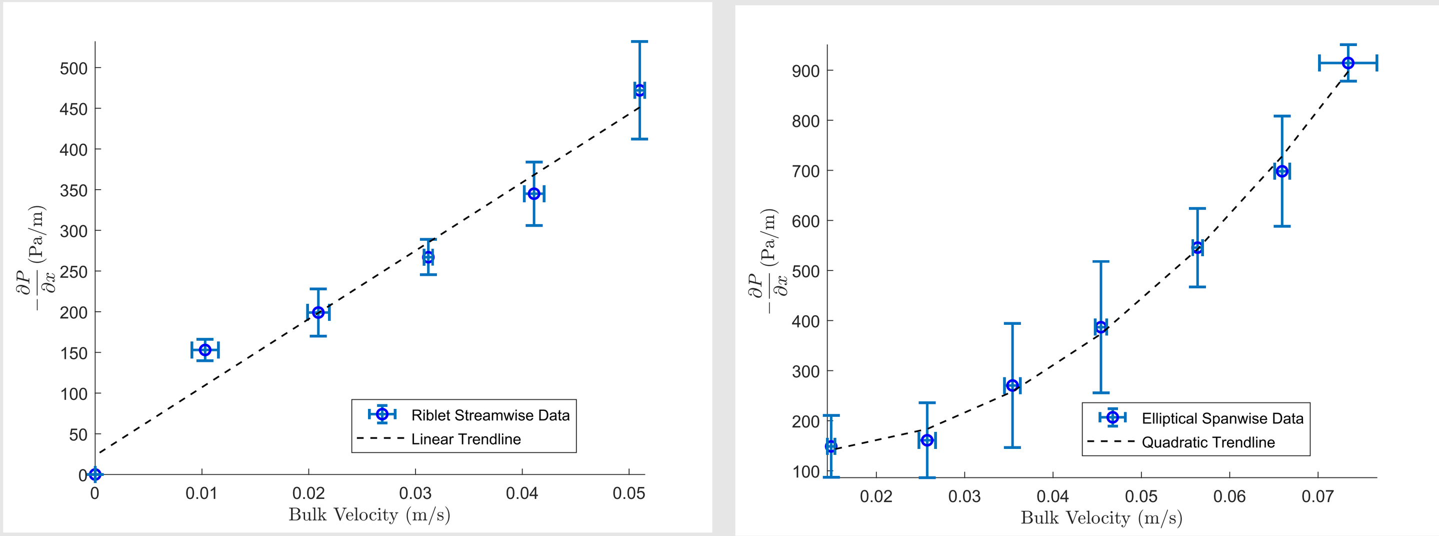

Figure 13. Some geometries portrayed a clear linear relationship (Riblet, left) between the pressure gradient and bulk velocity while others depicted a quadratic trend (Elliptical, right).

Geometry	K_{xx} (mm^2)	K_{yy} (mm^2)	K_{zz} (mm^2)	ϕ_{xy}	ϕ_{yz}	ϕ_{xz}
Trapezodial Riblets	0.22 ± 0.03	0.009 ± 0.002	0.061 ± 0.002	28 ± 10	0.14 ± 0.04	3.6 ± 0.5
Gyroid	0.06 ± 0.01	0.007 ± 0.001	0.018 ± 0.002	8 ± 2	0.4 ± 0.1	3.4 ± 0.7
Cubic	0.07 ± 0.03	0.05 ±0.03	0.05 ± 0.03	3 ± 2	2 ± 1	3 ± 2
Elliptical	0.05 ± 0.03	0.027 ± 0.008	0.027 ± 0.008	2 ± 1	1 ± 0.6	2 ± 1
Previous Experiments						
Cubic	0.07 ± 0.01	0.07 ± 0.01	0.07 ± 0.01	1 ± 0.3	1 ± 0.3	1 ±0.3

Table 1. Permeability values for the spanwise, streamwise, and wall normal directions as well as the anisotropy ratios (ϕ) for the geometries conducted. The cubic geometry permeability ratios concluded from previous experiments.

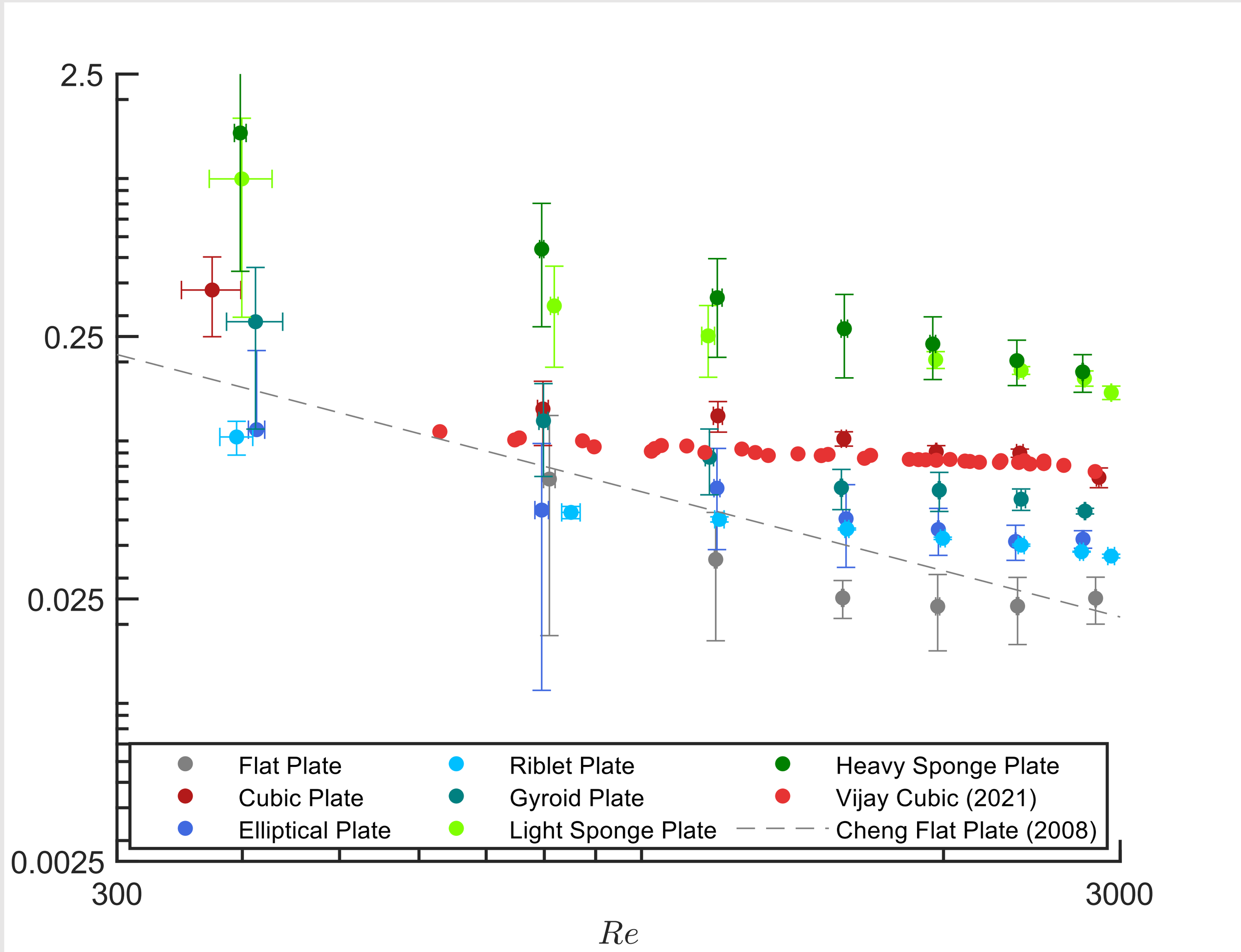

Figure 14. The large uncertainty at low Reynolds numbers is due to the limited resolution of the flowmeter and the pressure transducer. For higher Reynolds numbers, the expected decreasing trend of the friction factor matches theoretical predictions .

Conclusion

- As noted in figure 14 and table 1, the anisotropy of the structured geometries did not have a significant effect on the drag profiles at the Reynolds number tested. Based on the computational studies by Gomez and Garcia, the key factor in the reduction of drag is ϕ_{xy} under the condition that $\phi_{xy} = \phi_{xz}$. It is evident that for more complex structured geometries (i.e. trapezoidal and gyroid) the symmetry condition is not met, obscuring the relationship between anisotropy (ϕ_{xy}) and drag reduction.
- It is possible that the decreasing trend extends to higher Reynolds numbers and that the more anisotropic structures result in lower friction factors. From previous research, the friction factor asymptotically reaches a lower bound for Reynolds numbers larger than the ones tested. Therefore, experiments for Reynolds numbers >3000 need to be conducted to conclusively determine the relationship between anisotropy and friction factor.
- Based on the decreasing trend, two promising structures emerge: the gyroid and the riblet geometry. Further experiments altering the pore sizing along with testing at higher Reynolds numbers will illuminate more clearly whether the symmetry condition $\phi_{xy} = \phi_{xz}$ is plausible for more complex geometries and whether this criteria is conducive to drag reduction as expected from computational experiments.

References

[1] P. Ricco, M. Skote, M. A. Leschziner, "A review of turbulent skin-friction drag reduction by near-wall transverse forcing," Available: https://www.sciencedirect.com/science/article/abs/pii/S037604212100018X.

[2] Mubarak, A.K., and P.S. Tide. *Bonfring*, conference.bonfring.org/papers/gct_icmf2013/icmf234.pdf. Accessed 1 Dec. 2024.

[3] Hirt, G., and M. Thome. "Large Area Rolling of Functional Metallic Micro Structures - Production Engineering." *SpringerLink*, Springer-Verlag, 9 Nov. 2007, link.springer.com/article/10.1007/s11740-007-0067-z.

[4] [Endrikat, S., et al. "Influence of Riblet Shapes on the Occurrence of Kelvin–Helmholtz Rollers: Journal of Fluid Mechanics." *Cambridge Core*, Cambridge University Press, 2 Mar. 2021, www.cambridge.org/core/journals/journal-of-fluid-mechanics/article/abs/influence-of-riblet-shapes-on-the-occurrence-of-kelvinhelmholtz-rollers/CEA7823C0265742836CFC528CD429C05.

[5] G. Gomez-de-Segura, and R. Garcia-Mayoral, "Turbulent drag reduction by anisotropic permeable substrates - analysis and direct numerical simulations." Available: https://link.springer.com/article/10.1007/s10494-018-9916-4